Thermal Uniformity of 12-in Silicon Wafer During Rapid Thermal Processing by Inverse Heat Transfer Method

Senpuu Lin and Hsin-Sen Chu

Abstract—**Through an inverse heat transfer method, this paper presents a finite difference formulation for determination of incident heat fluxes to achieve thermal uniformity in a 12-in silicon wafer during rapid thermal processing. A one-dimensional thermal model and temperature-dependent thermal properties of a silicon wafer are adopted in this study. Our results show that the thermal nonuniformity can be reduced considerably if the incident heat fluxes on the wafer are dynamically controlled according to the inverse-method results. An effect of successive temperature measurement errors on thermal uniformity is discussed. The resulting maximum temperature differences are only 0.618, 0.776, 0.981, and 0.326 °C for 4-, 6-, 8- and 12-in wafers, respectively. The required edge heating compensation ratio for thermal uniformity in 4-, 6-, 8- and 12-in silicon wafers is also evaluated.**

Index Terms—**12-in silicon wafer, inverse heat-transfer method, rapid thermal processing, thermal uniformity.**

I. Introduction

As DEVICE dimension shrinks to the submicrometer range, reduction of thermal budget during microelectronic processing is becoming a crucial issue. Single-wafer rapid thermal processing (RTP) has become an alternative to the conventional furnace-based batch processing in many processes [1], [2]. To obtain uniform processing across the wafer and to prevent the creation of slip defects due to thermal stresses, the temperature must be nearly uniform on the wafer throughout the process cycle [3].

It is known that the incident heat flux profiles (the distribution of energy) from a RTP system must be nonuniform over a wafer to obtain uniform temperature at all times, the reason being heat loss by the edge of the wafer. Hill and Jones [4] investigated thermal uniformity with a uniform intensity field and one in which the intensity was linearly enhanced to a maximum of 8% vertically over the last 15 mm of a 6-in wafer. Kakoschke *et al.* [5] evaluated enhanced illumination intensities at wafer peripheries vertically and laterally for a compensation of edge heat losses during processing. Gyurcsik *et al.* [6] introduced a two-step procedure for solving an inverse optimal-lamp-contour problem to achieve temperature uniformity in steady state. Sorrel *et al.* [1] determined the increase in perimeter radiation required to maintain the wafer at approximately uniform temperature via applying power-law (first, second, and seventh degree) irradiant profiles. Norman [7] presented a technique based on linear programming for minimization of worst case error during temperature trajectory following. Zöllner *et al.* [8] compensated for radial temperature decreases using an adjustable lamp arrangement with optimized power settings calculated from wafer heat losses. Riley and Gyurcsik [9] determined the amount of lateral heating needed to counteract edge cooling during RTP. Cho *et al.* [10] optimized the incident heat flux profile over a wafer by determining the heat loss profiles using Lord's thermal model [3], which simulates radial temperature gradients by assuming uniform temperature through the wafer thickness. Following the work of Riley and Gyurcsik [9], Perkins *et al.* [2] used their special wafer-edge node analysis to show that idealized intensity profiles can maintain thermal uniformity at steady-state temperatures, and that dynamic continuously changing profiles are required to maintain temperature uniformity during thermal transients.

The works mentioned above describe quantifying incident heat flux over a wafer to achieve the necessary thermal uniformity requirement during RTP. However, the question is whether there is a more efficient way than a purely trial-and-error approach to determine the incident heat flux over a wafer to ensure thermal uniformity. The inverse heat transfer problems (IHTPs) deal with the determination of the crucial parameters in analysis such as the internal energy sources, surface heat fluxes, thermal properties, etc., and have been widely applied in many design and manufacturing problems [11]–[14]. The inverse source problem is practical in thermal uniformity of RTP systems in which the heat source strength required to achieve temperature uniformity is undetermined. The one-dimensional inverse problem with two unknown sources has been investigated, and satisfactory results are reported [15].

In this paper, a finite-difference solution to a one-dimensional (radius, assuming uniform temperature through the wafer thickness) thermal model in which both surfaces of a 12-in silicon wafer are heated is studied for application to RTP systems. The wafer is subjected to a steady uniformly distributed heat flux [2], [5] (uniform heat flux, i.e., intensity mode during processing). The temperature-dependent thermal properties of the silicon wafer are considered. Then, using the inverse heat transfer method [14], [15], the incident heat fluxes over the wafer required for thermal uniformity during ramp-up and steady-state phase of RTP are determined from known (desired or measured) wafer-center temperature trajectory.

Manuscript received November 22, 1999; revised April 14, 2000. This work was supported by the National Science Council, R.O.C., under Grant NSC 88-2218-E-009-003.

The authors are with the Department of Mechanical Engineering, National Chiao Tung University, Hsinchu, 300, Taiwan R.O.C. (e-mail: hschu@cc.nctu.edu.tw).

Publisher Item Identifier S 0894-6507(00)09494-X.

0894–6507/00$10.00 © 2000 IEEE

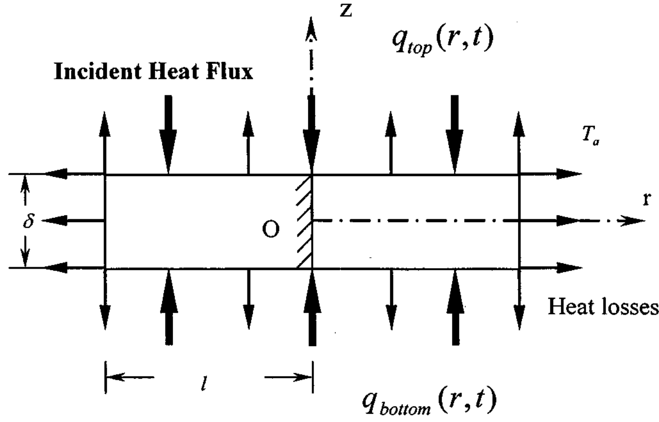

Fig. 1. Schematic representation of energy flux in a silicon wafer subjected to two-sided incident heat flux and heat losses emitted from all wafer surfaces.

The measurement-error effects on thermal uniformity are also discussed.

II. Thermal Model

Consider a thin axially symmetrical circular silicon wafer, as shown in Fig. 1. Let l and δ be the radius and thickness, respectively. T_0 is the initial temperature of the wafer, and the temperature of the surrounding medium is T_a. Symmetric heating on both sides of the wafer is assumed. The total incident heat fluxes on the top and the bottom surfaces of the wafer are represented by q_{top} and q_{bottom}, respectively. The heat losses occur at all wafer surfaces. Assume that the temperature is uniform through the wafer thickness. Thus a one-dimensional thermal model is adopted.

The governing equation for an axially symmetric cylindrical coordinate system with its origin at the wafer center is

$$\rho c(T)\frac{\partial T}{\partial t} = \frac{1}{r}\frac{\partial}{\partial r}\left[k(T)r\frac{\partial T}{\partial r}\right] + \frac{1}{\delta}[G_{\text{top}} + G_{\text{bottom}}], \qquad 0 < r < l \quad (1)$$

with

$$G_{\text{top}} = \alpha_{\text{top}} q_{\text{top}}(r,\, t) - \varepsilon_{\text{top}}\sigma_s(T^4 - T_a^4)$$
$$G_{\text{bottom}} = \alpha_{\text{bottom}} q_{\text{bottom}}(r,\, t) - \varepsilon_{\text{bottom}}\sigma_s(T^4 - T_a^4)$$

where $\sigma_s = 5.672 \times 10^{-12}$ Wcm^{-2}K^{-4} is Stefan–Boltzmann constant; wafer temperature T is a function of radius r and time t; and ρ, $k(T)$, $c(T)$, α_{top}, ε_{top}, α_{bottom}, $\varepsilon_{\text{bottom}}$ is wafer density, thermal conductivity, specific heat capacity, absorptivity of the top side, emissivity of the top side, absorptivity of the bottom side, and emissivity of the bottom side, respectively.

Note that the absorptivity and emissivity may depend on wafer temperature, position, and radiating spectral wavelength [16], [17]. And, because of the large temperature variations during processing, the temperature dependence of wafer thermal conductivity as well as specific heat capacity must be considered as follows [18]:

$$k(T) = 802.99\ \text{T}^{-1.12} \quad (\text{W cm}^{-1}\text{K}^{-1}) \quad 300 - 1683\text{K} \qquad (2a)$$

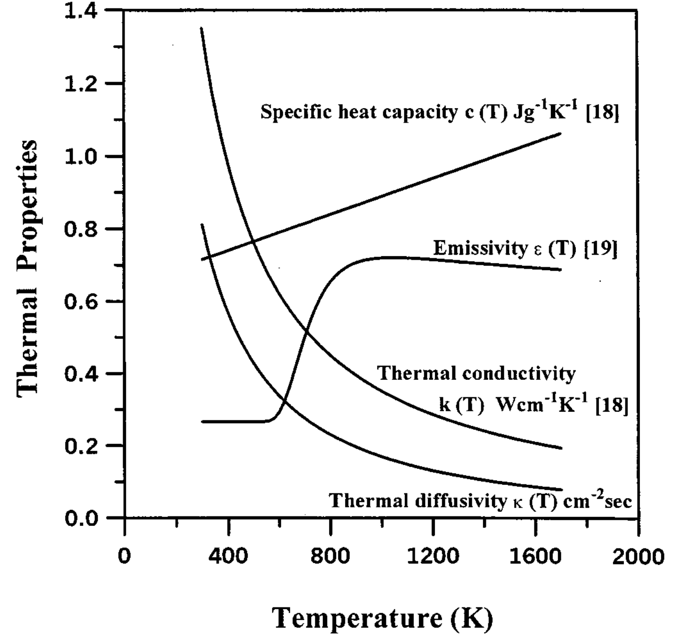

Fig. 2. Temperature-dependent thermal properties of a silicon wafer.

$$c(T) = 0.641 + 2.473 \times 10^{-4}\ \text{T} \quad (\text{J g}^{-1}\text{K}^{-1}) \quad >300\text{K} \qquad (2b)$$

while the wafer density is assumed to be constant and equal to 2.33 g-cm^{-3}. Since the silicon wafer is considered to be homogeneous in the present study, the dependence of $k(T)$ on spatial position is introduced implicitly only by the spatial dependence of the temperature. Because $k(T)$ is weakly dependent on temperature (see Fig. 2), spatial temperature variations across wafers at a certain time are expected to be small enough ($\leq$200 K) so that spatial variations in thermal conductivity may be ignored [5]. Equation (1) is thus reduced to

$$\rho c(T)\frac{\partial T}{\partial t} = k(T)\left[\frac{\partial^2 T}{\partial r^2} + \frac{1}{r}\frac{\partial T}{\partial r}\right] + \frac{1}{\delta}[G_{\text{top}} + G_{\text{bottom}}], \qquad 0 < r < l. \quad (3)$$

The initial and boundary conditions for the system mentioned above are

$$T(r,\, t) = T_i \qquad \text{at } t = 0 \quad (4)$$
$$\frac{\partial T}{\partial r} = 0 \qquad \text{at } r = 0 \quad (5)$$
$$-k(T)\frac{\partial T}{\partial r} = \varepsilon_{\text{edge}}\sigma_s(T^4 - T_a^4) \qquad \text{at } r = l \quad (6)$$

where $\varepsilon_{\text{edge}}$ is the emissivity for radiant heat loss emitted from the wafer edge. We may assume without loss of generality that the incident heat flux on both sides during processing is equal, i.e., $q_{\text{top}}(r,\, t) = q_{\text{bottom}}(r,\, t) = q(r,\, t)$, and that the absorptivity in all wafer surfaces is the same as the emissivity of these surfaces. For simplicity, the emissivity in all surfaces is assumed to be the same and only temperature dependence as [19]

$$\alpha_{\text{top}} = \varepsilon_{\text{top}} = \varepsilon_{\text{bottom}} = \alpha_{\text{bottom}} = \varepsilon_{\text{edge}} = \varepsilon(T) = 0.2662 + 1.8591T^{-0.1996}e^{-((1.0359\times 10^{25})/T^{8.8328})}. \quad (7)$$

Thus, (3) and (6) may be rewritten, respectively, as

$$\rho c(T)\frac{\partial T}{\partial t} = k(T)\left(\frac{\partial^2 T}{\partial r^2} + \frac{1}{r}\frac{\partial T}{\partial r}\right) + \frac{2}{\delta}\varepsilon(T) \cdot [q(r,t) - \sigma_s(T^4 - T_a^4)], \qquad 0 < r < l \tag{8}$$

and

$$-k(T)\frac{\partial T}{\partial r} = \varepsilon(T)\sigma_s(T^4 - T_a^4) \qquad \text{at } r = l. \tag{9}$$

The numerical solution techniques used here are from the finite-difference method. A central-difference representation of the space derivative and an implicit backward-difference representation of the time derivative are adopted. We can approximate the governing equation and the initial condition, as well as the boundary conditions, using $T(r, t) = \theta((i-1)\Delta R, n\Delta\tau) = \theta_i^n$ with p equidistant grid and the temporal coordinate increment $\Delta\tau$. After the nonlinear radiant fourth-power terms in (8) and (9) have been simulated using a linear scheme and the successive over-relaxation (SOR)-by-lines method has been adopted, the unknowns in the subgroups to be modified simultaneously are set up such that the matrix of coefficients will be tridiagonal in form permitting use of the Thomas algorithm as follows:

$$b_i^n\theta_{i-1}^n + d_i^n\theta_i^n + a_i^n\theta_{i+1}^n = c_i^n. \tag{10}$$

The superscript is denoted as the index of the temporal grid, and the subscript is denoted as the index of the spatial grid. Given the incident heat flux, we can obtain the wafer temperature distributions.

III. Inverse Heat Transfer Method

The inverse heat transfer problem in application to RTP is given a wafer temperature-distribution history to determine the incident heat flux profiles on the wafer required for achieving thermal uniformity during processing. The given wafer temperature-distribution history is just our desired temperature trajectory required for thermal uniformity. Without loss of generality, we may assume that the desired temperature trajectory is the temperature history of the wafer center as calculated from the thermal model given above using constant incident heat flux (uniform heat flux), i.e., intensity mode during processing [2], [5].

The finite-difference method in the thermal model above at $\tau = \tau^m = m\Delta\tau$ is used to construct the following matrix equation [14], [15]:

$$\lfloor F^m \rfloor\{\theta^m\} = \{\theta^{m-1}\} + \{S^m\} + \lfloor V^m \rfloor\{\varphi^m\}. \tag{11}$$

Then the temperature distribution $\{\theta^m\}$ can be derived as follows:

$$\begin{aligned}\{\theta^m\} &= [F^m]^{-1}\{\{\theta^{m-1}\} + \{S^m\}\} + [F^m]^{-1}[V^m]\{\varphi^m\} \\ &= [M^m]\{\{\theta^{m-1}\} + \{S^m\}\} + [N^m]\{\varphi^m\}\end{aligned} \tag{12}$$

where $[M^m] = [F^m]^{-1}$ and $[N^m] = [F^m]^{-1}[V^m]$.

The vector $\{\theta^{m-1}\}$ contains $p+1$ values of the initial distribution or the temperature distribution for the preceding time step. The vector $\{\varphi^m\}$ is composed by the unknown incident

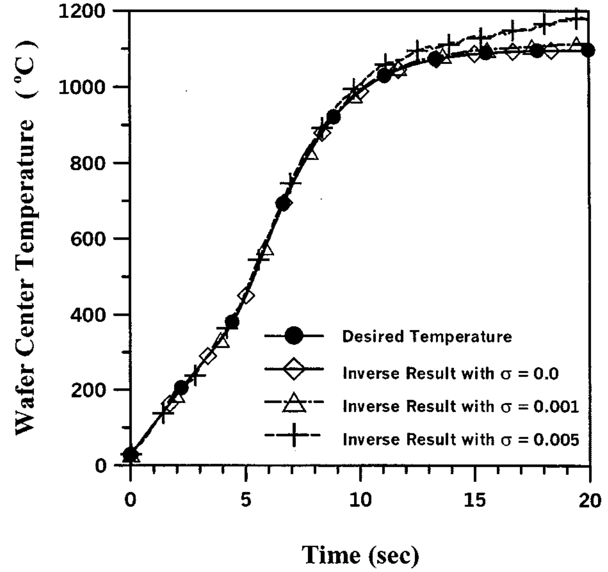

(a)

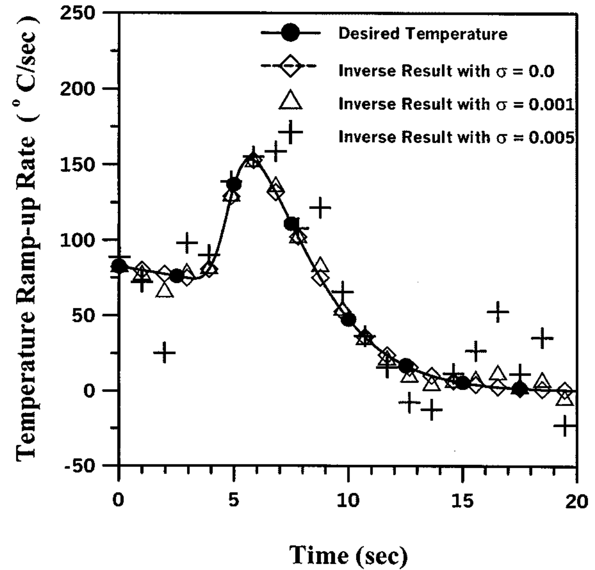

(b)

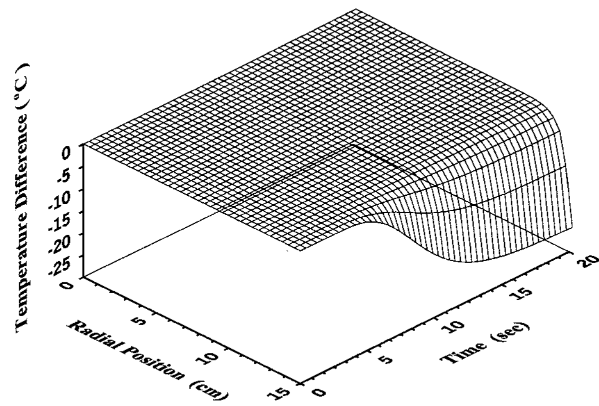

(c)

Fig. 3. (a) Desired temperature trajectory and inverse results for measurement errors $\sigma = 0.0$, $\sigma = 0.001$, and $\sigma = 0.005$. (b) Desired temperature ramp-up rate and inverse results for measurement errors $\sigma = 0.0$, $\sigma = 0.001$, and $\sigma = 0.005$. (c) Thermal distortions during uniform heat flux processing.

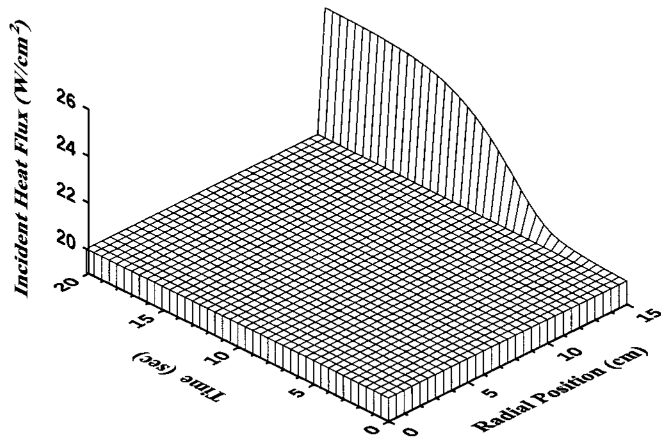

Fig. 4. Incident heat flux profile calculated by inverse method for measurement errors $\sigma = 0.0$.

heat fluxes φ_j^m for $j = 1, 2, \ldots, p, p+1$. As well, j is the grid number of the location of the estimated heat flux function φ_j. The vector $\{S^m\}$ includes any known variables of the problem, and the vector $\{V^m\}$ contains the coefficients for the unknown variables φ_j^m. A time-sequential procedure is used to determine the unknown incident heat flux parameters. The time domain is divided into analysis intervals, each of length $\tau^{m-1} \leq \tau \leq \tau^{m+r-1}$, where r is the number of future time steps [11]. The parameters φ_j^m are determined simultaneously for each analysis intervals.

For the next time step $m+1$, we arrive at

$$\begin{aligned}\{\theta^{m+1}\} &= [M^{m+1}]\{\{\theta^m\} + \{S^{m+1}\}\} + [N^{m+1}]\{\varphi^{m+1}\} \\ &= [M^{m+1}][M^m]\{\{\theta^{m-1}\} + \{S^m\}\} \\ &\quad + [M^{m+1}][N^m]\{\varphi^m\} + [M^{m+1}]\{S^{m+1}\}\} \\ &\quad + [N^{m+1}]\{\varphi^{m+1}\}. \end{aligned} \tag{13}$$

In the same way, the temperature distribution at successive r future times, $\tau = \tau^{m+r-1}$, can be represented as follows:

$$\begin{aligned}\{\theta^{m+r-1}\} &= [M^{m+r-1}]\{\{\theta^{m+r-2}\} + \{S^{m+r-1}\}\} \\ &\quad + [N^{m+r-1}]\{\varphi^{m+r-1}\} \\ &= [M^{m+r-1}][M^{m+r-2}]\cdots[M^{m+1}][M^m] \\ &\quad \cdot \{\{\theta^{m-1}\} + \{S^m\}\} + [M^{m+r-1}][M^{m+r-2}] \\ &\quad \cdots [M^{m+1}][N^m]\{\varphi^m\} \\ &\quad + [M^{m+r-1}][M^{m+r-2}]\cdots[M^{m+1}]\{S^{m+1}\} \\ &\quad + [M^{m+r-1}][M^{m+r-2}]\cdots[M^{m+2}][N^{m+1}] \\ &\quad \cdot \{\varphi^{m+1}\} + \cdots + [M^{m+r-1}]\{S^{m+r-1}\} \\ &\quad + [N^{m+r-1}]\{\varphi^{m+r-1}\}. \end{aligned} \tag{14}$$

To stabilize the estimated results in the inverse algorithms, a temporary assumption that the incident heat flux is constant over r future time steps is used

$$\varphi_j^{m+1} = \varphi_j^{m+2} = \cdots = \varphi_j^{m+r-1} = \varphi_j^m, \quad \text{for } j = 1, 2, \ldots, p, p+1. \tag{15}$$

Then, the temperatures θ_i^{m+k} at each i-spatial grid ($i = 1, 2, \ldots, p, p+1$) for each analysis interval

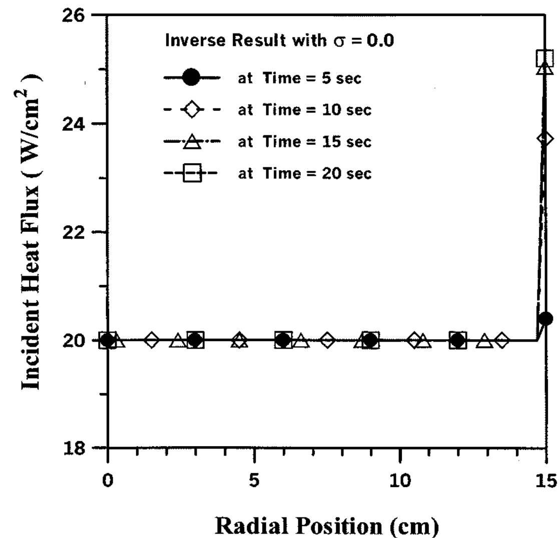

(a)

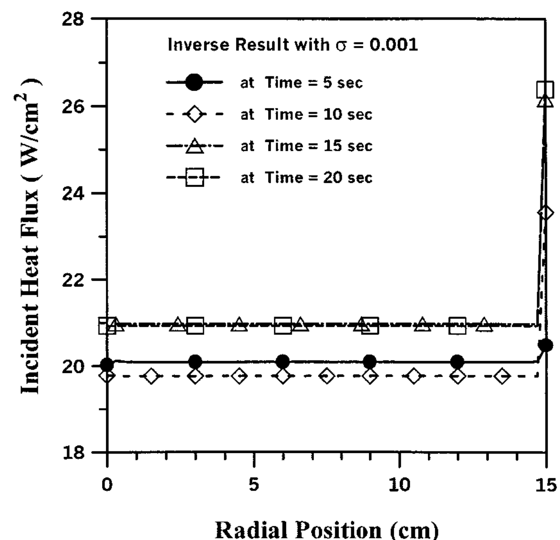

(b)

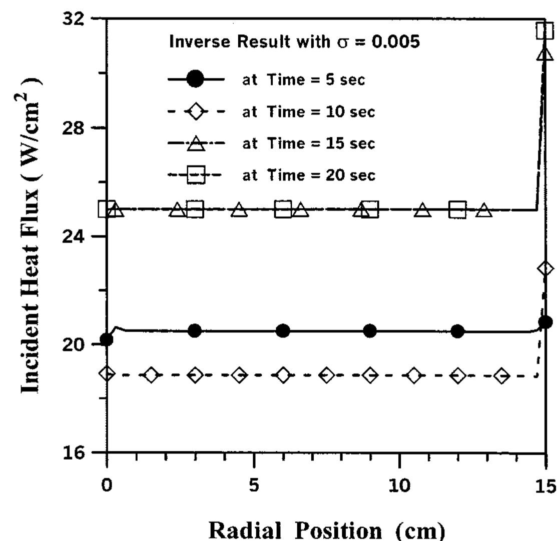

(c)

Fig. 5. Incident heat flux calculated by inverse methods at several times for measurement errors (a) $\sigma = 0.0$, (b) $\sigma = 0.001$, and (c) $\sigma = 0.005$.

$k = 0, 1, 2, \ldots, r-1$ can be derived. When $\tau = \tau^m$, the estimated parameter vectors $\{\varphi^1\}$, $\{\varphi^2\}$, ..., and $\{\varphi^{m-1}\}$ have been evaluated, and the task now is to determine the unknown incident heat flux vector $\{\varphi^m\}$. Thus, we can construct the following matrix equation:

$$\{\vartheta\}_{r\cdot(p+1)\times 1} = \{\Phi\}_{r\cdot(p+1)\times(p+1)}\{\Psi\}_{(p+1)\times 1}. \quad (16)$$

After the known temperature distributions are substituted into vector ϑ, the components of vector Ψ can be found using the linear least squares error method [20]. The result is

$$\Psi = (\Phi^T\Phi)^{-1}\Phi^T\vartheta. \quad (17)$$

This equation provides a sequential algorithm that can be used to estimate the unknown incident heat fluxes by increasing the value of m by one for each time step. Thereafter, the incident heat fluxes can be obtained iteratively along the temporal coordinate. The incident heat flux profiles on the silicon wafer required to maintain thermal uniformity during RTP can be determined from the desired temperature trajectories.

IV. Results and Discussion

The numerical solution techniques described above were used in a typical 12-in (775-μm thickness) silicon wafer. A simulation from initial temperature $T_0 = 27$ °C (300 K) transition over 20 s to a steady state of 1097 °C (1370 K) is demonstrated at the surrounding temperature $T_a = 27$ °C (300K) under the uniform incident heat flux $q(r, t) = 20$ W/cm^2. The assumptions of intensity mode and no reabsorption by the wafer itself were made during processing [2], [5]. The wafer center temperature and ramp-up rate were calculated by the finite-difference scheme during this temperature transition, as shown in Fig. 3(a) and (b), respectively, denoted by desired temperature, which was taken as the desired uniform temperature for the inverse calculation. Since there are no losses, also no intensity is required for compensation initially, and therefore all the absorbed energy is used to increase the wafer temperature. But, in this study, since the temperature-dependent absorptivity and emissivity are 0.3 at the initial lower temperature, and 0.68 from 800 K to 1700 K (see Fig. 2), there is a sharp increase at the temperature range 600 K–800 K, which is approximately 400 °C. The wafer is more efficient in energy absorption above this temperature. Thus, the wafer temperature rises more rapidly at this jump. As the wafer temperature increases with the increasing energy absorption, heat losses also increased as the wafer temperature increased and part of the absorbed energy is consumed for compensation. Accordingly, less absorbed energy is left for ramping. The ramp-up rate is decreased gradually. During the steady state, all the absorbed energy is consumed for compensating heat losses and nothing is left for ramping [5].

Fig. 3(c), a three-dimensional graph, shows temperature difference during uniform heat-flux processing. The axis "Radial Position" shows the distance from the wafer center in centimeters. The axis "Time" represents the time during this temperature transition. The vertical axis represents thermal nonuniformity graphed according to the temperature differences between points on the wafer and the wafer's center. The significant thermal gradients in the wafer undergoing this temperature transition were similar to the results reported by other authors [1]–[3]. Initially, the temperature difference developed near the wafer perimeter is small. Gradually, it becomes significant firstly at the wafer edge and increases with the time. Finally, when the wafer temperature approaches steady state, the greatest temperature difference of 25 °C occurs during this temperature transient.

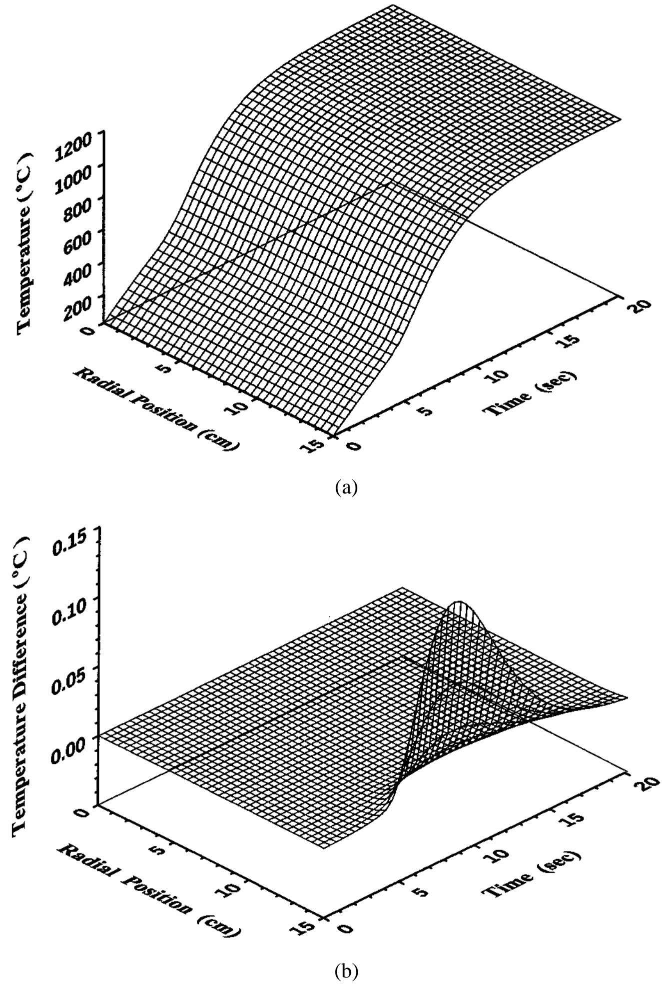

Fig. 6. Inverse results of (a) temperature distributions and (b) thermal distortions for measurement errors $\sigma = 0.0$.

In general, the temperature at the wafer center spot was monitored during the rapid thermal processing. The calculated temperature trajectory of the wafer center as shown in Fig. 3(a) was adopted as our desired (or measured) uniform temperature tracking required for thermal uniformity during processing. Since our desired (or measured) temperature trajectory was generated from the "exact" calculated finite-difference solutions described in Section II, it is presumed to contain errors for successive temperature measurement if there is an active temperature control. Random measurement errors may be added to the desired temperature trajectory in simulations, as described elsewhere [15]

$$Y_1^n = \theta_1^n + \omega\sigma \quad (18)$$

where the subscript "1" is the grid number of the spatial-coordinate at the wafer center and the superscript n denotes the

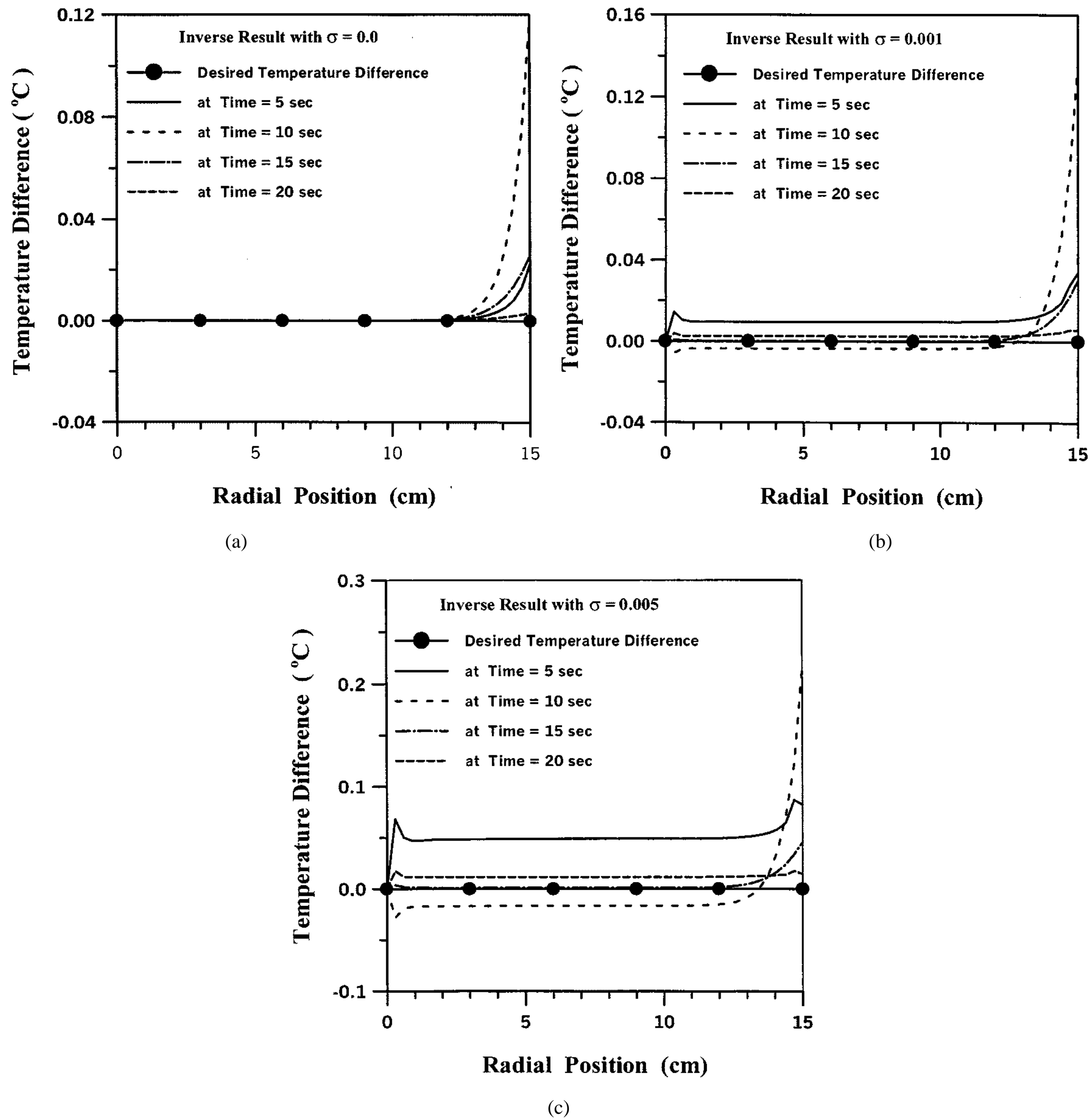

Fig. 7. Desired thermal uniformity and inverse results at several times for measurement errors (a) $\sigma = 0.0$, (b) $\sigma = 0.001$, and (c) $\sigma = 0.005$.

grid number of the temporal-coordinate. θ_1^n is the "exact" calculated temperature, Y_1^n is the "measured" temperature, σ is the standard deviation of measurement errors, and ω is a random number. The value of ω is calculated using the IMSL subroutine DRNNOR and chosen over the range $-2.576 < \omega < 2.576$, which represents the 99% confidence bound for the measurement temperature. For the cases of $\sigma = 0.001$ and $\sigma = 0.005$, in this study, the respective measured temperatures $\theta_1^n \pm 0.7728$ °C and $\theta_1^n \pm 3.864$ °C are simulated.

We set

$$Y_2^n = Y_3^n = \cdots = Y_p^n = Y_{p+1}^n = Y_1^n \tag{19}$$

as the requirement of thermal uniformity during rapid thermal processing, for our known temperature distribution θ_i^n used in the inverse heat-transfer method described in Section III to evaluate the incident heat flux φ_i^n profiles on the wafer. After the incident heat flux profiles for thermal uniformity were determined, the radial temperature distribution across the wafer was computed again using the finite-difference method described in Section II to make a comparison between the desired temperature distribution and the inverse-method results. The temperature trajectory and ramp-up rate calculated by inverse methods at the wafer center for measurement errors $\sigma = 0.0$ (means "exact"), $\sigma = 0.001$, and $\sigma = 0.005$ are also shown in Fig. 3(a) and (b). From this figure, we can see that estimation errors resulting from the measured errors are reasonable. The greater the measurement errors, the less accurate the estimated results. In the case of $\sigma = 0.0$, there is a good accuracy of estimated results through such an inverse heat transfer method.

Fig. 4 shows the three-dimensional graph of the incident heat-flux profiles calculated by inverse methods for measurement errors $\sigma = 0.0$ during processing. It is found that the heat compensation for thermal uniformity is only needed near the wafer edge. The result is similar to those reported

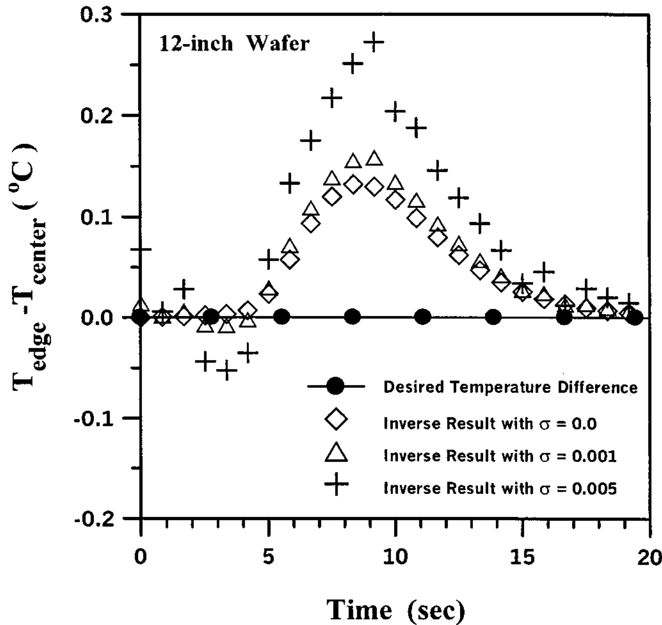

Fig. 8. Desired and inverse temperature-difference results between wafer edge and wafer center for measurement errors $\sigma = 0.0, \sigma = 0.001$, and $\sigma = 0.005$.

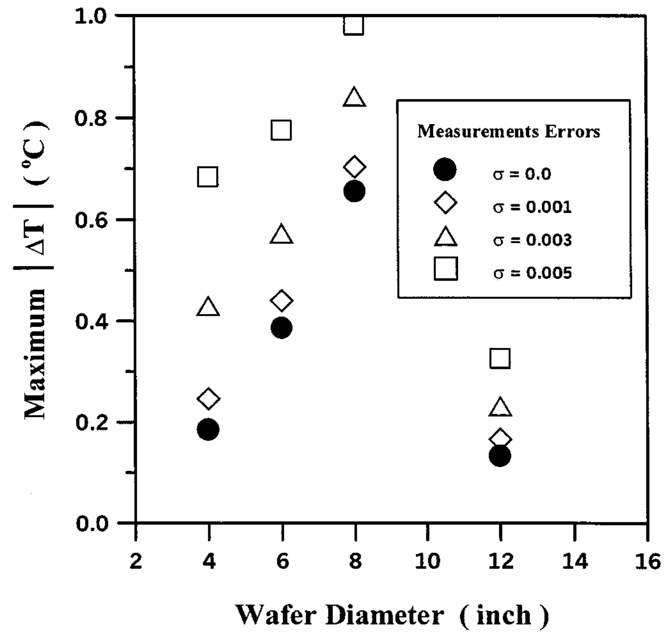

Fig. 9. Maximum temperature difference calculated by inverse method in the 4-, 6-, 8-, and 12-in silicon wafers for measurement errors $\sigma = 0.0, \sigma = 0.001$, $\sigma = 0.003$, and $\sigma = 0.005$.

by Perkins *et al.* [2]. During processing, the edge heating compensation increases with the increasing wafer temperature due to the increasing heat losses emitted from the wafer edge by fourth-power relationships with the temperature and temperature-dependent emissivity of the wafer. As the steady state is reached, the edge heating compensation is also to be constant. Fig. 5(a)–(c) shows the incident heat-flux profiles calculated by inverse methods at several times for measurement errors of $\sigma = 0.0$, $\sigma = 0.001$, and $\sigma = 0.005$, respectively. The only edge heating compensation for $\sigma = 0.0$ is also seen in Fig. 5(a). Since the measurement errors affect the given temperature trajectory during processing, in the case of $\sigma = 0.001$ [Fig. 5(b)] and $\sigma = 0.005$ [Fig. 5(c)], the incident heat flux profiles must be dynamically modulated with the measurement errors to maintain thermal uniformity in RTP systems. If it were not for the cooler edge of a wafer, thermal uniformity would be achieved by applying uniform heat flux profiles to the top or bottom surfaces of a wafer. However, because of the edge, the additional amounts of energy are directed to the edge for thermal uniformity, as shown in Figs. 4 and 5.

Fig. 6(a) shows a three-dimensional graph of the wafer temperature distributions calculated by inverse methods for measurement errors $\sigma = 0.0$ during processing. The thermal nonuniformity of temperature difference from wafer center calculated by inverse methods for measurement errors $\sigma = 0.0$ is demonstrated on Fig. 6(b). Initially, the thermal distortion developed at the wafer edge is small. As the wafer temperature increases, the thermal nonuniformity near the edge is increased with time. But the thermal nonuniformity can be decreased by the modulation of incident heat fluxes, and the wafer returns to thermal uniformity at the higher steady-state temperature of 1097 °C. Comparing with the uniform heat flux case in Fig. 3(c), we see that the maximum thermal distortion is reduced from 25 °C to 0.132 °C. Fig. 7(a)–(c) shows the temperature differences between points on the wafer and the wafer's center at several times for measurement errors of $\sigma = 0.0$, $\sigma = 0.001$, and $\sigma = 0.005$, respectively. For $\sigma = 0.0$, in Fig. 7(a), it also can be seen that the temperature difference is first developed at the wafer edge, and the evidence of the wafer's returning the thermal uniformity is also shown at the time of 20 s (near steady state). In Fig. 7(b) and (c), the thermal nonuniformity is developed at all surfaces, not from the edge. However, the maximum temperature difference occurs at the wafer edge. Fig. 8 shows the temperature differences between wafer edge and wafer center for several measurement errors during the processing. From these figures, we can find that the thermal nonuniformity increases with increasing measurement errors but remained under 0.3 °C when the incident heat fluxes on the wafer were dynamically varied according to the results calculated by inverse methods, although the dimensional measured error did reach 3.864 °C (in the case of $\sigma = 0.005$). The dynamic incident heat flux results yielded by the present inverse method show that thermal uniformity could be achieved efficiently during rapid thermal processing.

The dynamic incident heat flux calculated by inverse methods on thermal uniformity are also studied in 4-in (600-μm thickness), 6-in (675-μm thickness), and 8-in (725-μm thickness) silicon wafers. Fig. 9 shows the absolute value of maximum temperature difference from wafer center for these wafers in the temperature transients for measurement errors of $\sigma = 0.0$, $\sigma = 0.001$, $\sigma = 0.003$, and $\sigma = 0.005$, respectively. The most maximum temperature differences for measurement errors of $\sigma = 0.005$ are 0.618, 0.776, 0.981, and 0.326 °C for the 4-, 6-, 8-, and 12-in silicon wafers, respectively. The maximum temperature difference of 0.981 °C occurs in the case of

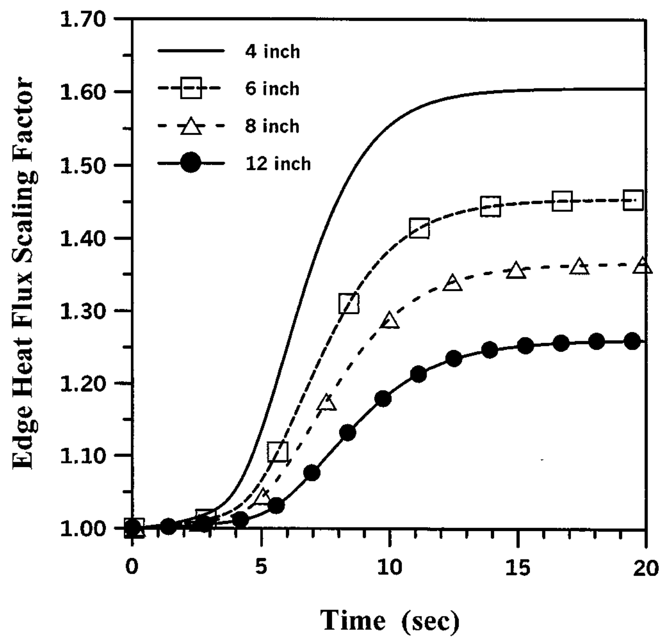

Fig. 10. Dynamic edge heating compensation scaling factors calculated by inverse method for 4-, 6-, 8-, and 12-inch silicon wafers.

the 8-in wafer. The 12-in wafer has the lowest maximum temperature difference. In the transient periods with measurement errors, the maximum temperature differences from wafer center remain under 1 °C.

Furthermore, as mentioned above, in the exact measurement errors of $\sigma = 0.0$, only edge heat compensation is needed to maintain thermal uniformity during processing. Following the works of Perkins *et al.* [2], we define the edge heat flux-scaling factor as the ratio of required edge compensation to uniform heat applied at central region. Fig. 10 shows the edge heat flux-scaling factor from the present results calculated by inverse methods for 4-, 6-, 8-, and 12-in wafers, respectively. Because edge heat radiant emission increased with the increasing wafer temperature, in the initial transient, the scaling factor increased with time. But when the energy of the incident heat fluxes finally balanced with the total energy emitted from the wafer, the wafer reached a constant temperature, referred to as the steady state, the scaling factor is independent of time. Since wafer thickness has increased much less than wafer diameter, the amount of radiant edge emission has not increased much, so the required edge heating ratio has decreased. If the edge heat flux can be controlled as shown in Fig. 10, thermal nonuniformity during processing can be reduced considerably. The maximum temperature differences in our study were 0.184, 0.385, 0.655 and 0.132 °C for 4, 6, 8, and 12 in, respectively, as shown in Fig. 9 for $\sigma = 0.0$.

V. Conclusion

Through an inverse heat-transfer method, this paper presents a finite difference formulation for the detection of unknown incident heat fluxes for achieving thermal uniformity in silicon wafer during RTP. A simulated 12-in silicon wafer subjected to a uniform heat flux of 20 W/cm^2 from 27 °C transition to a steady state of 1097 °C was studied at the surrounding temperature 27 °C. Our results show that the thermal nonuniformity can be reduced considerably if the incident heat fluxes on the wafer can be dynamically controlled according to the results calculated by inverse methods. Measurement error effects on the thermal uniformity were also discussed. The most maximum temperature differences in our study were 0.618, 0.776, 0.981, and 0.326 °C for 4-, 6-, 8-, and 12-in wafers, respectively. The maximum temperature difference occurred at the 8-in wafers. The 12-in wafer has the lowest maximum temperature difference. In the transient periods with measurement errors, the maximum temperature differences from wafer center were remained under 1 °C. The required edge heating compensation for thermal uniformity in 4-, 6-, 8-, and 12-in silicon wafers was also calculated using the inverse heat-transfer method. The maximum temperature differences in our study were only 0.184, 0.385, 0.655, and 0.132 °C for the 4-, 6-, 8-, and 12-in wafers, respectively.

References

[1] F. Y. Sorrell, M. J. Fordham, M. C. Öztürk, and J. J. Wortman, "Temperature uniformity in RTP furnaces," *IEEE Trans. Electron Devices*, vol. 39, pp. 75–79, Jan. 1992.

[2] R. H. Perkins, T. J. Riley, and R. S. Gyurcsik, "Thermal uniformity and stress minimization during rapid thermal processes," *IEEE Trans. Semiconduct. Manufact.*, vol. 8, pp. 272–279, Aug. 1995.

[3] H. A. Lord, "Thermal and stress analysis of semiconductor wafers in a rapid thermal processing oven," *IEEE Trans. Semiconduct. Manufact.*, vol. 1, pp. 105–114, Aug. 1988.

[4] C. Hill, S. Jones, and D. Boys, "Rapid thermal annealing—Theory and practice," in *Reduced Thermal Processing for ULSI, NATO ASI Series B: Physics*, 1989, pp. 143–180.

[5] R. Kakoschke, E. Bubmann, and H. Foll, "Modeling of wafer heating during rapid thermal processing," *Appl. Phys. A*, vol. 50, pp. 141–150, 1990.

[6] R. S. Gyurcsik, T. J. Riley, and F. Y. Sorrell, "A model for rapid thermal processing: Achieving uniformity through lamp control," *IEEE Trans. Semiconduct. Manufact.*, vol. 4, pp. 9–13, Feb. 1991.

[7] S. A. Norman, "Optimization of transient temperature uniformity in RTP systems," *IEEE Trans. Electron Devices*, vol. 39, pp. 205–207, Jan. 1992.

[8] J.-P. Zöllner, K. Ullrich, J. Pezoldt, and G. Eichhorn, "New lamp arrangement for rapid thermal processing," *Appl. Surf. Sci.*, vol. 69, pp. 193–197, 1993.

[9] T. J. Riley and R. S. Gyurcsik, "Rapid thermal processor modeling, control, and design for temperature uniformity," in *Proc. Mater. Res. Soc. Symp.* , vol. 303, 1993, pp. 223–229.

[10] Y. M. Cho, A. Paulraj, T. Kailath, and G. Xu, "A contribution to optimal lamp design in rapid thermal processing," *IEEE Trans. Semiconduct. Manufact.*, vol. 7, pp. 34–41, Feb. 1994.

[11] J. V. Beck, B. Blackwell, and C. R. St. Clair, *Inverse Heat Conduction—Ill-Posed Problem*. New York: Wiley, 1985.

[12] E. Hensel, *Inverse Theory and Applications for Engineers*. Englewood Cliffs, NJ: Prentice-Hall, 1991.

[13] O. M. Alifanov, *Inverse Heat Transfer Problems*. Berlin/Heidelberg, Germany: Springer-Verlag, 1994.

[14] K. Kurpisz and A. J. Nowak, *Inverse Thermal Problems*. Boston, MA: Computational Mechanics Publications, 1995, pp. 106–108.

[15] C.-Y. Yang, "The determination of two heat sources in an inverse heat conduction problem," *Int. J. Heat Mass Transfer*, vol. 42, pp. 345–356, 1999.

[16] J. P. Hebb and K. F. Jensen, "The effect of multilayer patterns on temperature uniformity during rapid thermal processing," *J. Electrochem. Soc.*, vol. 143, no. 3, pp. 1142–1151, Mar. 1996.

[17] P. Y. Wong, I. N. Miaoulis, and C. G. Madras, "Transient and spatial radiative properties of patterned wafers during thermal processing," in *Proc. Mater. Res. Soc. Symp.* , vol. 387, 1995, pp. 15–20.

[18] V. E. Borisenko and P. J. Hesketh, *Rapid Thermal Processing of Semiconductors*. New York: Plenum , 1997.

[19] A. Virzi, "Computer modeling of heat transfer in Czochralski silicon crystal growth," *J. Cryst. Growth*, vol. 112, pp. 699–722, 1991.

[20] G. Strang, *Linear Algebra and its Application*, 2nd ed. New York: Academic , 1980.

Senpuu Lin received the B.S. degree from National Cheng Kung University, Tainan, Taiwan, R.O.C., in 1979 and the M.S. degree from Lamar University, Beaumont, TX, in 1985, both in mechanical engineering, respectively. He is currently pursuing the Ph.D. degree in mechanical engineering at National Chiao Tung University, Hsinchu, Taiwan, R.O.C.

Since 1986, he has been an Instructor with National Lien Ho Institute of Technology, Miao-Li, Taiwan. His research interests include heat transfer problem by inverse methods and semiconductor manufacturing.

Hsin-Sen Chu was born in Hsinchu, Taiwan, R.O.C., on June 12, 1952. He received the B.S., M.S., and Ph.D. degrees from National Cheng Kung University, Tainan, Taiwan, in 1974, 1977 and 1982, respectively, all in mechanical engineering.

Presently, he is a Professor in the Department of Mechanical Engineering, National Chiao Tung University (NCTU), Hsinchu, Taiwan. He joined the NCTU Faculty in 1984. From 1985 to 1986, he was a Visiting Scholar at University of California, Berkeley. His current research interests are concerned with the heat transfer in semiconductor manufacturing, microscale heat transfer, and energy engineering.

Dr. Chu received the Outstanding Teaching Award sponsored by the Ministry of Education, R.O.C., in 1992.